*C*atalytic activation via π –backbonding in halogen bonds?

Andrew Wang[a,‡] and Pierre Kennepohl[*a,b]

The role of halogen bonding (XB) in chemical catalysis has largely involved using XB donors as Lewis acid activators to modulate the reactivity of partner Lewis bases. We explore a more uncommon scenario, where a Lewis base modulates reactivity via a spectator halogen bond interaction. Our computational studies reveal that spectator halogen bonds may play an important role in modulating the rate of S_N2 reactions. Most notably, π acceptors such as PF_3 significantly decrease the barrier to subsitution by decreasing electron density in the very electron rich transition state. Such π-backbonding represents an example of a heretofor unexplored situation in halogen bonding: the combination of both σ-donation and π-backdonation in this "non-covalent" interaction. The broader implications of this observation are discussed.

Introduction

Applications of halogen bonding and other forms of secondary interactions[1] have increased dramatically in the last decade. The reversible, yet highly directional, halogen bond (XB) has been used successfully in crystal engineering,[2–4] supramolecular chemistry,[5,6] selective binding and sensing[7–10], and medicinal chemistry.[11] More recently, they have been applied towards chemical catalysis.[12–14] Many examples of XB activation for chemical processes have focused on developing highly electron-deficient *XB* donors[Note 1] (the electron acceptor, i.e. the Lewis acid A-X, Figure 1) that modulate the reactivity of *XB acceptors* (the electron donor, i.e., the Lewis base D). In such cases, the catalyst acts as a classical Lewis acid catalyst. Examples of Lewis base catalysis where an A-X moiety acts as the target for activation are rare. To our knowledge, literature examples are limited to stoichiometric activation, such as those demonstrated in perfluoroalkylation reactions.[12,15,16]

XBs have typically been described to involve a σ -type electrostatic interaction due to the presence of a zone of electron deficiency at the apex of a terminal halogen atom, termed the σ-hole. The region of positive electrostatic potential leads to an attractive force between the halogen and electron-rich molecules, i.e. good Lewis bases. However, the exact nature of such XB interactions has led to significant debate in the literature. Valence electronic absorption and X-ray absorption spectroscopy have been interpreted within the context of molecular orbital (MO) representations of bonding and, within this framework, reveal strong covalent contributions in many halogen bonds.[17–20] For this reason, we have argued that XBs are more analogous to coordination bonds than to the typically-used analogy to hydrogen bonds.[21] By contrast, it has been argued that covalency (or charge transfer) models relying on MO descriptions are indistinguishable from charge polarization phenomena.[22–26] Given the prevalence of MO theory as a framework for the interpretation of chemical phenomena, and its widespread implementation in general quantum chemical tools, we feel that describing XB interactions using charge transfer/covalency – especially within the context of chemical reactivity– is both appropriate and useful.[27] One major benefit of the MO formalism is the convenience and power of differentiating between different types of donor/acceptor interactions, *i.e.*, separating σ/π/δ-type bonding contributions. Notably, π-type bonding in XB interactions was recently observed both computationally[28] and experimentally.[29] Exploring the relevance and importance of such contributions in halogen bonding is only just beginning.

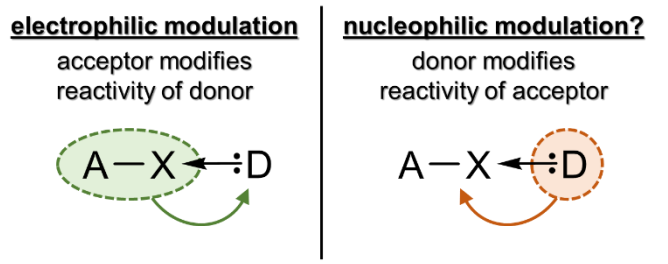

Figure 1. Simplified view of different modes of activation in XB-assisted catalysis. On the left, we depict electrophilic modulation (the most common motif in the literature), where the acceptor (A-X) is the catalyst, which modulates the reactivity of the donor (D). The opposite strategy involves using a catalytic donor (D) to modulate the reactivity of the acceptor (A-X). Here, donor and acceptor refer to those for electrons (see Note 1).

Herein, we use density functional methods to explore electronically different donors to mediate chemical reactivity via *secondary* halogen bonding, i.e. where the halogen involved in XB is not directly involved in the chemical reaction. We use simple prototypical S_N2 reactions to probe the effect of halogen bonding to a spectator iodine atom in geminal diiodomethanes. We find that spectator XB interactions can either raise or lower the activation energy of the substitution depending on the electronic properties of the Lewis base. A prototypical σ-donor only such as NH_3 leads to an increased activation barrier for S_N2, whereas a π-acceptor such as PF_3 *lowers the activation barrier*. These results reveal that π-backbonding may serve as a pathway for stabilization of the transition state in S_N2 reactions.

We chose to explore symmetric self-exchange S_N2 reactions to simplify the overall process (Scheme 1). Geminal diiodomethanes allow for one spectator iodine to be involved in XB throughout the reaction and one reactive iodine. Using a

[a] *Department of Chemistry, The University of British Columbia, 2036 Main Mall, Vancouver, British Columbia, Canada.*
[b] *Department of Chemistry, University of Calgary, 2500 University Drive NW, Calgary, Alberta, Canada.*
‡ *Current address: Department of Chemistry, University of Toronto, 80 St. George Street, Toronto, Ontario, Canada*

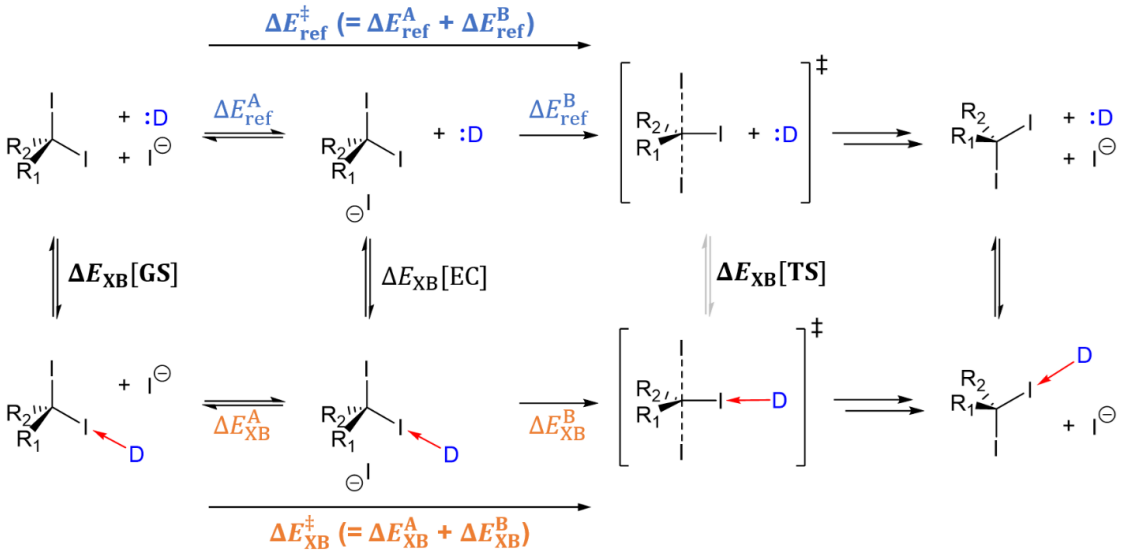

Scheme 1. Thermodynamic scheme for the symmetric self-exchange S_N2 reaction in the absence (top) and presence (bottom) of XB donor-acceptor interactions. Energies calculated include both enthalpies (E = H) and free energies (E = G). A series of different substitution patterns (R_1, R_2) were chosen to take account of other possible electronic contributions (see Note 2 for details). Four different donors were used in this study: NH_3, CO, PF_3, and PH_3.

range of substituents with differing electronic properties (R_1/R_2 = H, CH_3, CN, @Cy[Note 2]) helps us establish that any observed XB effect is due to effects from the electron donor and not due to substituent effects on the diiodomethane.

Results & Discussion

Symmetric self-exchange S_N2 reactions often have a double well reaction profile, which includes both the formation of the encounter complex and substitution itself (Scheme 1). Energies for species in the ground state (GS), encounter complex (EC), and at the transition state (TS) were calculated. As expected, the enthalpy of stabilization due to halogen bonding (ΔH^{o}_{XB}) is typically negative due to a favourable donor-acceptor interaction, whereas ΔG^{o}_{XB} is positive due to entropy.[5] Notably, we focus our attention on enthalpic contributions in this analysis due to our interest in the role of electronic contributions to the observed processes. Gibbs free energy results are provided for completeness in the Electronic Supplementary Information (ESI). We note here that since we are interested in the *changes in the activation barrier* going from no XB to XB, the entropic factor for XB formation (specifically the electron donor term) cancels out in the corresponding calculations, allowing the changes in the enthalpy of activation ($\Delta\Delta H^{\ddagger}$) to be a suitable parameter to describe the effect of XB on the reaction barrier. We also show in Figure S1 that results from $\Delta\Delta G^{\ddagger}$ are similar to those obtained for $\Delta\Delta H^{\ddagger}$.

We define the reaction barrier from separated reactants to the transition state (see Figure 1).[30] This simplifies our analysis and allows us to avoid some of the specific complexities related to the encounter complex itself.[31] The effect of halogen bonding in the ground state is particular easy to quantify and thus provides a more convenient reference point. The effect of spectator XB interactions on the reaction barrier are defined as the difference between the enthalpy of activation in the presence of XB ($\Delta H^{\ddagger}_{XB}$) and the enthalpy of activation without XB ($\Delta H^{\ddagger}_{ref}$) such that $\Delta\Delta H^{\ddagger} = \Delta H^{\ddagger}_{XB} - \Delta H^{\ddagger}_{ref}$. $\Delta\Delta H^{\ddagger}$ can also expressed as the difference between the XB stabilization of the GS (ΔH^{o}_{XB}[GS]) and that of the TS (ΔH^{o}_{XB}[TS]), *i.e.*, $\Delta\Delta H^{\ddagger} = \Delta H^{o}_{XB}[TS] - \Delta H^{o}_{XB}[GS]$. This is convenient in that it allows us to consider three regimes depending on the value of $\Delta\Delta H^{\ddagger}$:

(A) $\Delta\Delta H^{\ddagger} > 0$ *i.e.* $|\Delta H^{o}_{XB}[TS]| > |\Delta H^{o}_{XB}[GS]|$

(B) $\Delta\Delta H^{\ddagger} \approx 0$ *i.e.* $|\Delta H^{o}_{XB}[TS]| \approx |\Delta H^{o}_{XB}[GS]|$

(C) $\Delta\Delta H^{\ddagger} > 0$ *i.e.* $|\Delta H^{o}_{XB}[TS]| < |\Delta H^{o}_{XB}[GS]|$

Figure 2 illustrates $\Delta\Delta H^{\ddagger}$ as plots of $\Delta H^{\ddagger}_{XB}$ vs. $\Delta H^{\ddagger}_{ref}$. The dashed line corresponds to the situation where $\Delta H^{\ddagger}_{XB} = \Delta H^{\ddagger}_{ref}$; data above that line represent $\Delta\Delta H^{\ddagger} > 0$ and those below the line $\Delta\Delta H^{\ddagger} > 0$. When CO is the donor,[Note 1] the entire series of geminal diiodomethanes fall along the reference line such that $\Delta\Delta H^{\ddagger} \approx 0$. CO has little effect on the reaction barrier. For a stronger donor, such as NH_3, we find that the data generally fall in the regime where $\Delta\Delta H^{\ddagger} > 0$, and thus the XB interaction has a deleterious influence on the kinetics of substitution.[Note 3] By contrast, PF_3 has the opposite effect ($\Delta\Delta H^{\ddagger} < 0$) and is predicted to accelerate substitution. The effect is quite pronounced with an average stabilization of ~10 kJ/mol), and is also observed using $\Delta\Delta G^{\ddagger}$ (see Figure S1).

The dramatically different behaviour of NH_3 and PF_3 donors in their influence on the substitution reaction required further scrutiny. Below, we evaluate differences in both the ground state and transition state halogen bonding in each of these cases in order to identify the origin of this effect.

XB in the ground state – We employed the natural bond orbital (NBO) formalism to evaluate contributions to the XB interactions. Correlation plots between ground state thermodynamic data and σ-type halogen bonding contributions (via 2nd order perturbation analysis of the $LP_{donor} \rightarrow \sigma^{*}_{C-I[XB]}$ interaction[Note 4]; $E^{(2)}[\sigma^{*}]$) are shown in Figure S2 (top). For both CO and NH_3, a good correlation is obtained between the strength of σ donation and the overall stabilization obtained via halogen bonding (ΔH^{o}_{XB}[GS]). For PF_3 we find that while the electron donor forms an adduct with the diiodomethane, the XB interaction is very weak (< 2 kJ/mol) and there is a weak

anticorrelation with $E^{(2)}[\sigma^*]$. The calculated P-I bond distances are very close to the sum of their Van der Waals radii, thus PF_3 is acting as a very poor donor.[5]

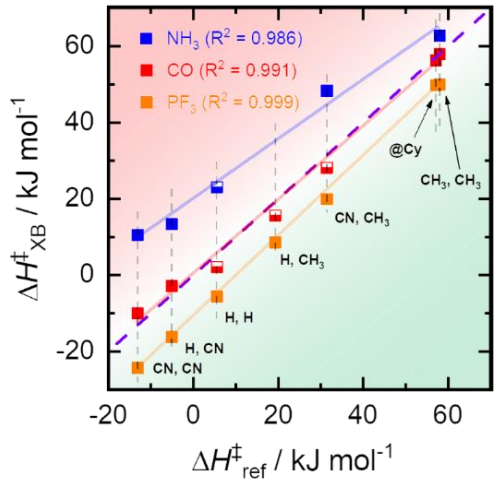

Figure 2. $\Delta H^{\ddagger}_{XB}$ vs. $\Delta H^{\ddagger}_{ref}$ with PF_3 (orange), CO (red), and NH_3 (blue) as the electron donor. The purple dashed line serves as a reference for $\Delta H^{\ddagger}_{XB} = \Delta H^{\ddagger}_{ref}$. Data above the line implies $\Delta H^{\ddagger}_{XB} > \Delta H^{\ddagger}_{ref}$ such that $\Delta\Delta H^{\ddagger} > 0$, and data below the line implies $\Delta H^{\ddagger}_{XB} < \Delta H^{\ddagger}_{ref}$ such that $\Delta\Delta H^{\ddagger} < 0$, with the vertical distance from each data point to the purple dashed line representing the absolute value of $\Delta\Delta H^{\ddagger}$. The sets of substituents are in the form (R_1, R_2). Half-filled squares for CO indicate the presence of additional (small) imaginary frequencies in the TS, and for NH_3 a small imaginary frequency in the ground state (see Tables S6 and S9). (H, CH_3) and (@Cy) not plotted for NH_3 as no XB is present in the TS for those cases. See Figure S1 for $\Delta G^{\ddagger}$.

XB in the transition state – Similar correlation plots in the transition state are shown in Figure S2 (bottom) for all three donors. In all cases, $\Delta H^{o}_{XB}[TS] < 0$. As in the ground state data, correlations are observed with $E^{(2)}[\sigma^*]$ for CO and NH_3. PF_3 yet again behaves differently and shows no correlation with $E^{(2)}[\sigma^*]$ even though thermodynamic stabilization from halogen bonding is now significant (~10 kJ/mol).

We also examined the influence of XB interactions on calculated TS structures. There were few significant changes with CO as a donor, but the effects are quite pronounced – and very different – in NH_3 and PF_3. The amine donor leads to an expansion of the TS, *i.e.*, the bond distances between the electrophilic carbon and the terminal iodides *are more elongated* in the presence of the spectator halogen bond (see Figure S2b). Conversely, the halogen-bonding to the phosphine leads to contraction of the TS, *i.e.*, these same bonds *are more contracted* when the donor is PF_3 (see Figure S2a). This effect also correlates with changes in charge distribution within the TS structure. One would typically expect charge donation via halogen bonding to increase electron density in the acceptor via $D \rightarrow \sigma^*_{C-I[XB]}$ donation, leading to increased Pauli repulsion in the acceptor. This is observed with the amine donor, causing an expansion of the transition state structure. However, one observes the opposite with the phosphine donor. The contraction suggests depletion of electron density at the electrophilic carbon.

It is well-known that PF_3 acts as a strong π-acceptor in transition metal chemistry,[32] providing a potential rationale to the observed behaviour. To evaluate this possibility, we examined changes in atomic charges from natural population analysis (NPA)[33] in the presence/absence of XB interactions (see Section 1 of ESI). Changes in NPA charges across the system allows for estimates of charge redistribution due to halogen bonding. The largest effect of PF_3 binding is a decrease in electron density in the two terminal iodides, with a concomitant increase in the perpendicular "C-I···PF_3" fragment. The effect of the other substituents is minor. Charge accumulation is particularly large in the halogen-bonded iodine atom and the F atoms in PF_3.

The data for NH_3 indicate different charge redistribution upon halogen bonding in the transition state. We find increasing charge density ($\Delta q < 0$) along the primary I-C-I axis, reflecting charge donation from the amine towards the central carbon atom, leading to elongation of the terminal C-I bonds and charge localization at the termini (see ESI Section 1.2). Using CO as the Lewis base results in very small changes in bond distances and concurrently more ambiguous changes in charge redistribution (see ESI Section 1.3). Taken together, the data can be summarized as shown in Scheme 2: strong σ donation from NH_3 leads to deactivation, a combination of weak but balanced σ donation/π backdonation from CO cancel each other out, and relatively weak σ donation and strong π backdonation from PF_3 leads to activation.

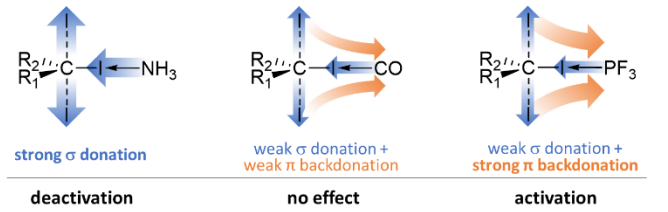

Scheme 2. Schematic representation of charge flow in each of the transition state structures.

This perspective is supported by evaluation of the canonical molecular orbitals in the XB-assisted transition state. It has previously been shown that the orbitals involved in the three-centre four-electron bond that form the S_N2 TS are of the proper symmetry to be affected by substituents with the appropriate π-type symmetry, and such interactions can lead to an increase or decrease of the activation barrier of the substitution.[34] Inherently, the spectator iodo substituent isn't completely innocent, as its filled 5p valence orbitals leads to Pauli repulsion and should destabilize the transition state. The presence of a π-acidic phosphine in the appropriate orientation, however, provides a pathway to funnel excess electron density away from the I-C-I core, decrease repulsion, and stabilize the transition state. Moreover, the filled I_{5p} orbitals on the terminal iodides may also form combinations of appropriate symmetry with the spectator iodo substituent, and thus with the appropriate phosphine π acceptor orbitals. This interaction would typically reflect Pauli repulsion of the iodines, but the π-type pathway towards the PF_3 relieves this repulsion and funnels electron density towards the terminal fluorine atoms. A total of three π-type MOs can contribute to backbonding as described above, and one additional weaker interaction is observed perpendicular to the CI_3 plane (Figures 3a and S17). All of these

are stabilized due to the presence of the XB interaction in the transition state to a larger extent than the overall valence stabilization that results from electron redistribution from the electron rich TS to the electron-poor PF_3 group (Figure 3b, see Section 3.5 of ESI for details). The isotropic influence of the donor is reflected in the energy of frontier density of states of the TS (TDOS, see Figure 3c and S19): as expected, the amine donor destabilizes the frontier orbitals through charge donation into an already electron rich system, whereas the phosphine donor lowers the TDOS envelope through the π-type pathways described previously.

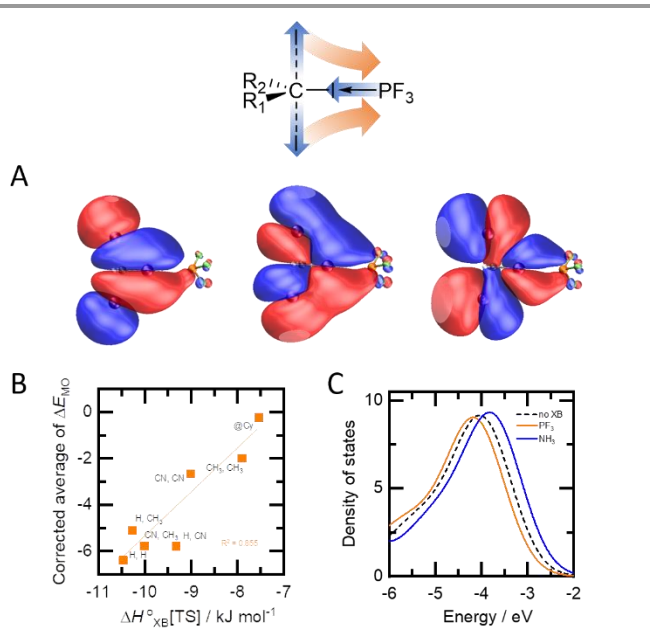

Figure 3. Orbital analysis of the PF_3 backbonding interaction in the transition state: A) Most important π-type MOs contributing to backbonding, represented with (R_1, R_2) = (H, H); see Figure S17 for other complexes. B) Average changes of the π-type MO energies going from no XB to XB (ΔE_{MO}), corrected against a reference *d*-orbital on the incoming iodide, plotted against $\Delta H^{\circ}_{XB}[TS]$ for PF_3 as the electron donor. C) Gaussian-broadened total density of states around the highest occupied MO (HOMO) for the set (H, H) with no XB (dashed line), PF_3 as the electron donor (orange line), and NH_3 as the electron donor (blue line). See Figure S19 for all sets.

In a final attempt to challenge our assertion that π-backbonding is the critical factor in the XB interaction with phosphines, we attempted similar calculations with PH_3, which is a very poor π-acceptor compared to PF_3.[32] In all cases but one, XB interactions in the TS could not be identified.[Note 5]

Results from this study clearly indicate dramatically different behaviour depending on the electronic nature of the donor used to modulate the substitution reaction. Changes in both geometry and charge distribution lead to the conclusion that one may significantly alter reaction kinetics by changing the nature of the Lewis base. As we observe through this study, a base that is simultaneously a poor σ-donor and a good π-acceptor is most beneficial to lower the barrier for an electron rich S_N2 reaction. In the ground state, PF_3 may only act as a poor σ-donor, and thus has only a weak influence on the overall system. Increased electron density in the transition state and the required geometric changes enable efficient π-backdonation, which stabilizes the transition state. By contrast, the situation for NH_3 is deleterious rather than beneficial because it more strongly stabilizes the ground state molecule than the transition state. CO is generally considered to be a strong π-acceptor and we might expect that it could behave similarly to PF_3 in the transition state, however we postulate that poor orbital overlap with the large valence 5*p* orbitals on the iodine is responsible for its poor ability in this situation.

Conclusions

This systematic study of a prototypical S_N2 reaction illustrates the potential role of specific orbital interactions in influencing reactivity via halogen bonds. The weak σ-donor and strong π-acceptor character of PF_3 stabilizes the transition state and has a pronounced effect on the predicted rates of substitution. This behaviour strengthens our contention that one may consider halogen bonds in a manner similar to transition metal coordination bonds,[21,29] with electronic interactions of different symmetry playing different roles depending on the inherent electronic nature of the donor/acceptor pair. We demonstrate one example where this behaviour can used to modulate reactivity and propose that further investigations are warranted. We suggest that rational design of halogen bonding catalysts – with appropriate inclusion of π contributions – should be explored.

Conflicts of interest

There are no conflicts of interest to declare.

Acknowledgements

The authors would like to thank UBC Chemistry, WestGrid, and Compute Canada for computational resources used for this work.

Methods

All calculations were performed using the Gaussian 09 software[35] with molecules built in WebMO.[36] For all calculations, the M06-2X functional[37] was used owing to its excellent performance on describing thermochemical kinetics and intermolecular interactions.[37,38] The aug-cc-pVDZ-PP basis set (parameters obtained from the ESML basis set exchange[39,40]) was used for iodine and jun-cc-pVDZ[41] for all other elements. All calculations were performed in the gas phase, at 298.15 K, and 1 atm using an ultrafine integration grid (99 radial shells, 590 angular points).

Ground state structures were optimized to a minimum from a starting distance of ~3 Å between the donor and acceptor atoms and an initial XB angle of ~180 degrees, then followed by frequency calculations for the thermochemical data (calculated from the electronic energies (Section 4 of ESI) according to ref. 42), and to verify the absence of imaginary frequencies.

Transition state calculations were first performed without XB, with an initial search for the transition state via a relaxed potential energy surface scan along the reaction coordinate (distance between the incoming iodide and the electrophilic carbon), then optimized with the Berny algorithm.[43–47] The QST2 algorithm[48] was used when the Berny algorithm fails to produce an accurate transition state structure. Frequency

calculations are then carried out for the thermochemical data and to verify the presence of exactly one imaginary frequency with the vibrational mode corresponding to substitution of LG by Nu along the reaction coordinate. TS structures with XB were optimized from an initial configuration consisting of the optimized TS of the geminal iodide and the electron donor placed at a distance of ~ 3 Å between the donor and acceptor atoms and an initial XB angle of ~180 degrees, followed by the same procedure for optimizing the TS without XB.

From the optimized structures, MO calculations were performed, and NBO and NPA calculations were carried out with the NBO package built into Gaussian 09. Gaussian-broadened density of states were calculated using Multiwfn via the Hirshfield method.[49] MO cube files (~512 000 grid points) were generated using Multiwfn, rendered using the Visual Molecular Dynamics software [50], and traced with POV-Ray 3.6.[51]

Notes

1. We choose the convention of donor/acceptor as would be used to describe ligands in transition metal chemistry, i.e. a donor is an electron donor and an acceptor in an electron donor. This is unfortunately in conflict with common XB terminology that borrows from that used in hydrogen bonds.

2. We adopt the shorthand (R_1, R_2) in the text to describe the substituents on each diiodomethane. R_1 and R_2 involve all combinations of H, CH_3, and CN, and @Cy refers to a cyclohexane ring, taking up the positions of R_1 and R_2, with the electrophilic carbon as part of the ring.

3. For NH_3 with the sets of substituents (H, CH_3) and (@Cy), we were unable to obtain a TS structure with XB, hence the absence of data for those substituents.

4. I[XB] refers to the iodine directly involved in XB.

5. For all substituents in the series except (@Cy), where $\Delta H^{o}_{\mathrm{XB}}[\mathrm{TS}] \approx$ -4 kJ/mol, there was either no XB or we were unable to obtain converged calculations.

References

1 R. H. Crabtree, *Chem. Soc. Rev.*, 2017, **46**, 1720–1729.
2 A. Mukherjee, S. Tothadi and G. R. Desiraju, *Acc. Chem. Res.*, 2014, **47**, 2514–2524.
3 J. Teyssandier, K. S. Mali and S. De Feyter, *ChemistryOpen*, 2020, **9**, 225–241.
4 Ö. D. Ateş, Y. Zorlu, S. D. Kanmazalp, Y. Chumakov, A. G. Gürek and M. M. Ayhan, *CrystEngComm*, 2018, **20**, 3858–3867.
5 L. C. Gilday, S. W. Robinson, T. A. Barendt, M. J. Langton, B. R. Mullaney and P. D. Beer, *Chem. Rev.*, 2015, **115**, 7118–7195.
6 P. Metrangolo, F. Meyer, T. Pilati, G. Resnati and G. Terraneo, *Angew. Chem. Int. Ed.*, 2008, **47**, 6114–6127.
7 M. J. Langton, S. W. Robinson, I. Marques, V. Félix and P. D. Beer, *Nat. Chem.*, 2014, **6**, 1039–1043.
8 J. Y. C. Lim, T. Bunchuay and P. D. Beer, *Chem. - Eur. J.*, 2017, **23**, 4700–4707.
9 B. R. Mullaney, A. L. Thompson and P. D. Beer, *Angew. Chem. Int. Ed.*, 2014, **53**, 11458–11462.
10 R. Hein, A. Borissov, M. D. Smith, P. D. Beer and J. J. Davis, *Chem. Commun.*, 2019, **55**, 4849–4852.
11 R. Wilcken, M. O. Zimmermann, A. Lange, A. C. Joerger and F. M. Boeckler, *J. Med. Chem.*, 2013, **56**, 1363–1388.
12 R. L. Sutar and S. M. Huber, *ACS Catal.*, 2019, **9**, 9622–9639.
13 S. Kuwano, T. Suzuki, M. Yamanaka, R. Tsutsumi and T. Arai, *Angew. Chem. Int. Ed.*, 2019, **58**, 10220–10224.
14 D. Bulfield and S. M. Huber, *Chem. - Eur. J.*, 2016, **22**, 14434–14450.
15 R. Beniazza, L. Remisse, D. Jardel, D. Lastécouères and J.-M. Vincent, *Chem. Commun.*, 2018, **54**, 7451–7454.
16 F. Sladojevich, E. McNeill, J. Börgel, S.-L. Zheng and T. Ritter, *Angew. Chem. Int. Ed.*, 2015, **54**, 3712–3716.
17 S. V. Rosokha, C. L. Stern and J. T. Ritzert, *Chem. - Eur. J.*, 2013, **19**, 8774–8788.
18 S. V. Rosokha and M. K. Vinakos, *Phys Chem Chem Phys Phys Chem Chem Phys*, 2014, **16**, 1809–1813.
19 S. V. Rosokha, *Faraday Discuss*, 2017, **203**, 315–332.
20 S. W. Robinson, C. L. Mustoe, N. G. White, A. Brown, A. L. Thompson, P. Kennepohl and P. D. Beer, *J. Am. Chem. Soc.*, 2015, **137**, 499–507.
21 C. L. Mustoe, D. Yu, M. Gunabalasingam, B. O. Patrick and P. Kennepohl, *Faraday Discuss.*, 2017, **203**, 79–91.
22 T. Clark, *Faraday Discuss*, 2017, **203**, 9–27.
23 T. Clark, J. S. Murray and P. Politzer, *Aust. J. Chem.*, 2014, **67**, 451–456.
24 P. Politzer, J. S. Murray and T. Clark, *J. Mol. Model.*, 2015, **21**, 52.
25 T. Brinck and A. N. Borrfors, *J. Mol. Model.*, 2019, **25**, 125.
26 T. Clark, J. S. Murray and P. Politzer, *Phys. Chem. Chem. Phys.*, 2018, **20**, 30076–30082.
27 P. R. Varadwaj, A. Varadwaj and H. M. Marques, *Inorganics*, 2019, **7**, 40.
28 S. J. Ang, A. M. Mak and M. W. Wong, *Phys. Chem. Chem. Phys.*, 2018, **20**, 26463–26478.
29 C. W. Kellett, P. Kennepohl and C. P. Berlinguette, *Nat. Commun.*, 2020, **11**, 3310.
30 T. A. Hamlin, M. Swart and F. M. Bickelhaupt, *ChemPhysChem*, 2018, **19**, 1315–1330.
31 M. Stei, E. Carrascosa, M. A. Kainz, A. H. Kelkar, J. Meyer, I. Szabó, G. Czakó and R. Wester, *Nat. Chem.*, 2016, **8**, 151–156.
32 M. P. Mitoraj and A. Michalak, *Inorg. Chem.*, 2010, **49**, 578–582.
33 A. E. Reed, R. B. Weinstock and F. Weinhold, *J. Chem. Phys.*, 1985, **83**, 735–746.
34 D. Kost and K. Aviram, *Tetrahedron Lett.*, 1982, **23**, 4157–4160.
35 Gaussian 09, Revision D.01, M. J. Frisch, G. W. Trucks, H. B. Schlegel, et al., Gaussian, Inc., Wallingford CT, 2013.
36 J. R. Schmidt and W. F. Polik, WebMO Enterprise, version 20.0, WebMO LLC, Holland, MI, USA, 2020.
37 Y. Zhao and D. G. Truhlar, *Theor. Chem. Acc.*, 2008, **120**, 215–241.
38 A. J. Cohen, P. Mori-Sánchez and W. Yang, *Chem. Rev.*, 2012, **112**, 289–320.
39 D. Feller, *J. Comput. Chem.*, 1996, **17**, 1571–1586.
40 K. L. Schuchardt, B. T. Didier, T. Elsethagen, L. Sun, V. Gurumoorthi, J. Chase, J. Li and T. L. Windus, *J. Chem. Inf. Model.*, 2007, **47**, 1045–1052.
41 E. Papajak, J. Zheng, X. Xu, H. R. Leverentz and D. G. Truhlar, *J. Chem. Theory Comput.*, 2011, **7**, 3027–3034.
42 J. W. Ochterski, Gaussian, Inc., Wallingford CT, 2000.
43 H. Bernhard Schlegel, *Theor. Chim. Acta*, 1984, **66**, 333–340.
44 J. Simons, P. Joergensen, H. Taylor and J. Ozment, *J. Phys. Chem.*, 1983, **87**, 2745–2753.
45 A. Banerjee, N. Adams, J. Simons and R. Shepard, *J. Phys. Chem.*, 1985, **89**, 52–57.
46 J. Baker, *J. Comput. Chem.*, 1986, **7**, 385–395.
47 J. Baker, *J. Comput. Chem.*, 1987, **8**, 563–574.
48 C. Peng and H. Bernhard Schlegel, *Isr. J. Chem.*, 1993, **33**, 449–454.
49 T. Lu and F. Chen, *J. Comput. Chem.*, 2012, **33**, 580–592.
50 W. Humphrey, A. Dalke and K. Schulten, *J. Mol. Graph.*, 1996, **14**, 33–38.
51 Persistence of Vision Pty. Ltd., Persistence of Vision Raytracer (Version 3.6), 2004, http://www.povray.org/download/.